Available online at www.sciencedirect.com
SCIENCE DIRECT®
ELSEVIER
Nuclear Instruments and Methods in Physics Research A 519 (2004) 687–694
NUCLEAR INSTRUMENTS & METHODS IN PHYSICS RESEARCH Section A
www.elsevier.com/locate/nima

Image reconstruction and material Z discrimination via cosmic ray muon radiography

L.J. Schultz[a,b,*], K.N. Borozdin[a], J.J. Gomez[a], G.E. Hogan[a], J.A. McGill[c], C.L. Morris[a], W.C. Priedhorsky[a], A. Saunders[a], M.E. Teasdale[a,d]

[a] *Physics Division, Los Alamos National Laboratory, Bikini Atoll Road, P-25/MS H846, Los Alamos, NM 87544, USA*
[b] *Portland State University, Portland, OR 97201, USA*
[c] *General Atomics, San Diego, CA 92186, USA*
[d] *University of Rhode Island, Kingston, RI 02881, USA*

Received 3 July 2003; received in revised form 18 September 2003; accepted 14 October 2003

Abstract

Highly penetrating cosmic ray muons shower the Earth at the rate of 10,000 $m^{-2}\,min^{-1}$ at sea level. In our previous work (Nature 422 (2003) 277; Rev. Sci. Instr. 74(10) (2003) 4294; Cosmic Ray Muon Radiography for Contraband Detection, in: Proceedings of AccApp'03, San Diego, CA, June 2003), we presented a novel muon radiography technique which exploits the multiple Coulomb scattering of these particles for nondestructive inspection without the use of artificial radiation. In this paper, we describe the concept of and theory behind cosmic ray muon radiography. We discuss the information carried by the scattered muons and our approaches for exploiting that information with image reconstruction algorithms. We discuss preliminary and advanced reconstruction algorithms, which take advantage of the scattering angle, scattering location, and locations where strongly scattered muons cross paths. Our algorithms are validated with both experimental demonstrations and Monte Carlo simulations. Based upon the results from both the experiment and simulations, we conclude that scattering muon radiography can be useful for both material discrimination and fast (minute order) detection of compact high-Z objects. Our ray-crossing algorithm, which highlights locations where strongly scattered muons cross paths, is effective even in the presence of a medium-Z background matrix.

PACS: 13.85.Tp; 81.70.Tx

Keywords: Cosmic rays; Muons; Radiography; Tomography; Contraband detection

1. Introduction

When cosmic rays strike the Earth's atmosphere, a cascade of many types of subatomic particles is created. Hadronic particles produced in the shower either interact or decay, and electrons and photons lose energy rapidly through pair production and Bremsstrahlung so that by the time this shower of particles reaches the Earth's surface, it is comprised primarily of muons. The flux reaching the surface of the Earth is about 10,000 muons per minute per square meter [1]. The mean energy of muons at sea level is about

*Corresponding author.
E-mail address: schultz@lanl.gov (L.J. Schultz).

0168-9002/$ - see front matter © 2003 Elsevier B.V. All rights reserved.
doi:10.1016/j.nima.2003.11.035

3–4 GeV, sufficient to penetrate meters of rock. Making practical use of these free particles is an attractive idea. As the spectrum of the muons is continuous and the average range is long, differential attenuation can be used to radiograph large objects. E.P. George made the first such effort in 1955 [2]. George measured the depth of rock above an underground tunnel by making use of the attenuation of cosmic ray muons. He measured the attenuated cosmic ray flux inside the tunnel and the incident flux outside the tunnel and inferred the rock depth from the ratio of these signals. Luis Alvarez followed George's work with his radiography of the Second Pyramid of Giza in 1970 [3], again using attenuation of the cosmic ray flux. In subsequent years, several researchers have used the attenuation of cosmic rays to make measurements on large structures or geographic objects. Minato [4] used cosmic ray counts to radiograph a large temple gate. Nagamine et al. [5] continue active research into the prediction of volcanic eruptions through cosmic ray attenuation radiography. Frlez et al. [6] recently reported using tomographic methods to track the passage of cosmic rays muons through cesium iodide crystals for quality control purposes.

The topic of this paper is a new form of cosmic ray muon radiography that is based on the multiple Coulomb scattering of the particles as they pass through material. By using multiple scattering instead of attenuation as the information source, we are able, in principle, to produce radiographs of objects of any thickness through which a sufficient number of muons survive to achieve the desired precision. The use of passive cosmic ray muons allows us to radiograph dense objects *with no artificial dose of radiation*. We introduced this technique in Ref. [7], and discussed its potential application to detection of high-Z objects in low-density surroundings in Refs. [8,9]. Herein, we describe the details of the theory, experimental demonstration, and reconstruction algorithms and provide some illustrative results.

2. Cosmic ray muons and multiple scattering

The cosmic ray muon flux may be described in terms of rate per unit area and time, and depends on particle momentum and arrival angle. Many researchers have measured and documented the cosmic ray flux (e.g. [10,11]). The surface spectrum varies with altitude, geophysical location, and other factors, but experimentalists often refer to the following "rules of thumb" to describe the muon spectrum [1]: (1) The momentum distribution is almost flat for momenta below 1 GeV, and falls as $p^{-2.7}$ for momenta above 10 GeV. The mean muon momentum is about 3–4 GeV. (2) The flux is greatest at the zenith, and falls approximately as $\cos^2(\theta)$, where θ is plane angle from vertical. (3) The overall muon rate is about $10{,}000\,\mathrm{m}^{-2}\,\mathrm{min}^{-1}$ for horizontal detectors.

Muons passing through material lose energy due to ionization, and may range out if their energy approaches zero. This absorption provides the information source used by George, Alvarez, and others as described in Refs. [2–5]. A muon passing through material is also deflected by many small-angle scatters off of the nuclei of the material. As illustrated in Fig. 1, the particle will traverse the material in a stochastic path due to these multiple scatters. The muon emerges from the material at an aggregate scattered angle θ, displaced from the unscattered exit point by a distance x. The angular scattering distribution is approximately Gaussian (the distribution has long tails, but the central 98% is well described as Gaussian), with zero mean and a standard deviation for scattering in the plane given by [1]:

$$\sigma_\theta = \frac{13.6\,\mathrm{MeV}}{\beta c p}\sqrt{\frac{L}{L_0}}\left[1 + 0.038\ln\left(\frac{L}{L_0}\right)\right] \tag{1}$$

where p is the momentum, and βc the velocity of the incident particle ($\beta c = 1$ for muons). L is the depth of the material, and L_0 is the radiation length of the material. The distribution of ray displacement in the plane may also be approximated as a Gaussian, with standard deviation:

$$\sigma_x = \frac{L}{\sqrt{3}}\sigma_\theta. \tag{2}$$

In addition, scattering angle and ray displacement are correlated, with correlation coefficient:

$$\rho_{\theta x} = \frac{\sqrt{3}}{2}. \tag{3}$$

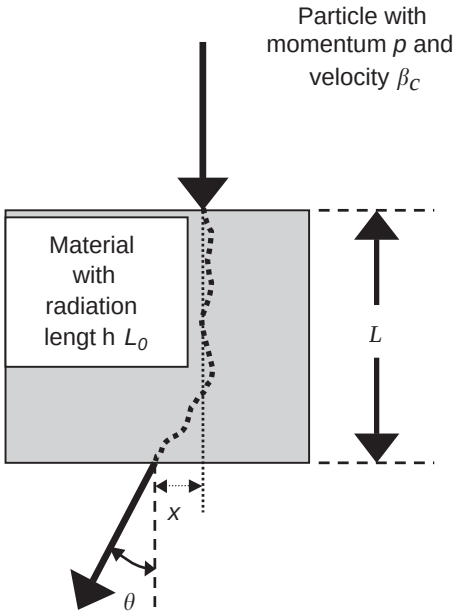

Fig. 1. Multiple Coulomb scattering of a charged particle through material. The magnitude of scattering is exaggerated for illustrative purposes.

Finally, the scattering into a plane orthogonal to x is independent and identically distributed to the scattering in x.

Radiation length, the characteristic range for scattering and other electromagnetic interactions, decreases with increasing material Z number. The mean scattering angle for a given material depth therefore increases with Z, according to Eq. (1), as illustrated in Fig. 2. This Z sensitivity, coupled with the long range of muons, makes muon scattering of particular interest as an information source for the detection of high-Z material in low-Z surroundings.

3. Material identification from muon scattering

For our purposes, we will define "material identification" as discrimination between low-Z (water, plastic, concrete), medium-Z (iron, copper), and high-Z (lead, tungsten, uranium) materials. As the scattering of muons in these three groups differs significantly (see Fig. 2), we can

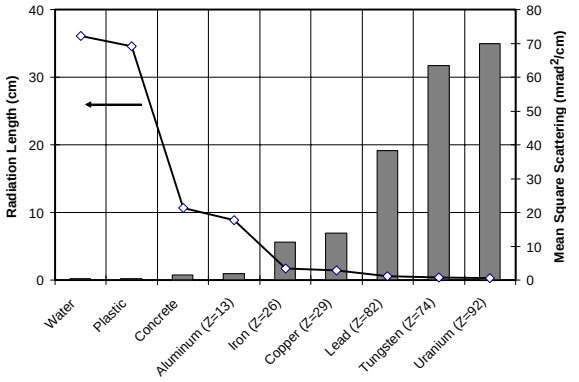

Fig. 2. Radiation length and mean square scattering per unit depth of 3 GeV muons (denoted as "scattering strength" in the text) through various materials, showing dependence on material Z number.

approximate the mean scattering angle by dropping the logarithmic term in Eq. (1) with little error.

$$\sigma_\theta \cong \frac{13.6}{p}\sqrt{\frac{L}{L_0}}. \tag{4}$$

We then establish a nominal muon momentum (3 GeV, for example), and define the *mean square scattering of nominal muons per unit depth* of a material as

$$\lambda_{\mathrm{mat}} = \left(\frac{13.6}{p_0}\right)^2 \frac{1}{L_{0,\mathrm{mat}}} \cong \sigma^2_{\theta_0,\mathrm{mat}}. \tag{5}$$

This parameter, which we will call the "scattering strength", depends only on material radiation length, and varies strongly with material Z, as shown in Fig. 2. We use the scattering strength to discriminate materials.

To infer the composition of a test object by measuring the scattering of N muons passing through that object, we can estimate the scattering strength by simply calculating momentum normalized mean square scattering. If, for each muon, we measure scattering in two orthogonal planes x and y, and if we know the path length L_i and the momentum p_i of each muon through the material:

$$\hat{\lambda} = \frac{1}{N}\sum_{i=1}^{N}\left(\frac{p_i^2}{p_0^2}\cdot\frac{\theta_{xi}^2+\theta_{yi}^2}{2L_i}\right). \tag{6}$$

It is easily shown that the uncertainty in our estimate is

$$\frac{\Delta\lambda}{\lambda} \cong \sqrt{\frac{1}{N}}. \tag{7}$$

For a 10 cm cube of material, we expect about 100 muons in a minute of exposure, and the one sigma uncertainty in our estimate of scattering strength is 10%.

More realistically, we will have at best an estimate of particle momentum, $\hat{p}$. If we know the momentum to an uncertainty of $\Delta p/p = E_p$, we must modify Eq. (6) to remove bias introduced by the variance of the momentum estimate:

$$\hat{\lambda} = \frac{1}{N(1+E_p^2)} \sum_{i=1}^{N} \left(\frac{\hat{p}_i^2}{p_0^2} \frac{\theta_{xi}^2 + \theta_{yi}^2}{2L_i} \right) \tag{8}$$

and the uncertainty in the scattering strength will increase over that expressed in Eq. (7). In the next section, we will discuss a simple method to estimate the momentum, and show the effect on our estimate of the scattering strength.

4. Momentum estimation and the cosmic ray muon radiography concept

In the previous section, we discussed the identification of a single isolated piece of material. More generally, we wish to infer the contents of an unknown volume that could contain many different materials.

Our concept is shown in Fig. 3. Muons pass through two position-sensitive detectors above an object volume, providing incoming angle and position. They then pass through the object volume and are scattered to an extent dependent upon the material through which they pass. The position and angle of scattered particles are measured in a lower pair of detectors. Each detector measures particle position in two orthogonal coordinates, so we obtain two scattering measurements from each particle. We show the object volume overlaid with a grid to signify our intent to reconstruct a discrete estimate of the scattering strength within the object volume.

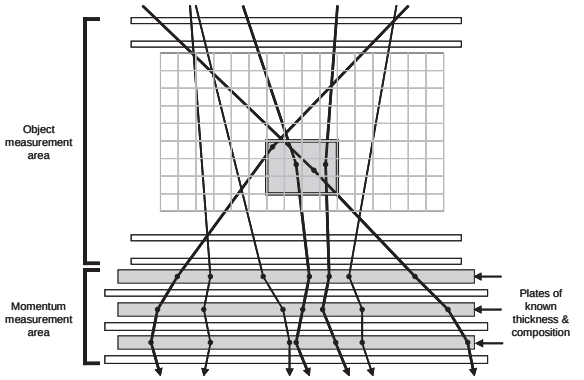

Fig. 3. Cosmic ray muon radiography concept. In the upper section, scattering of muons is used to identify unknown material. In the lower section, scattering of muons through known material is used to infer muon momentum.

Below the object measurement area, we place a sandwich of detectors and plates of known material and thickness. By measuring particle scattering through these plates, we can estimate particle momentum. We obtain two scattering measurements per plate. It can be shown that, if we make M scattering measurements to estimate momentum, the expected scattering strength uncertainty is

$$\frac{\Delta\lambda}{\lambda} \cong \sqrt{\frac{1}{N}} \sqrt{\frac{M-1}{M-4}}, \quad M > 4. \tag{9}$$

This uncertainty when $M = 4$ is theoretically infinite when the range of potential muon momenta is infinite. We find through simulation using about 1,000,000 muons drawn from a distribution as in Ref. [10] that uncertainty in the $M = 4$ case is typically about twice that of the $M = 6$ case. In any event, for a 10 cm cube we previously calculated an uncertainty of 10% in the inferred scattering strength for 1 min of exposure and perfect knowledge of momentum using Eqs. (6) and (7). If, instead, we estimate momentum using three scattering plates, the uncertainty increases to 16% according to Eqs. (8) and (9), still a reasonable figure for segregating low-, medium-, and high-Z materials.

For example, consider three blocks, one of concrete, one of iron, and one of uranium. We will assume 100 particles in 1 min of exposure, and

use three scattering plates for momentum estimation. For the concrete block, we expect a scattering strength of about 1.6, with 3 sigma confidence intervals of [0.8, 2.3]. The confidence intervals for the iron block are [5.9, 16.5], and for the uranium block [36.7, 103.1]. We can clearly segregate the three blocks in 1 min.

5. Three-dimensional object reconstruction: the PoCA algorithm

For our first demonstrations of muon radiography, we developed a simple, intuitive algorithm. The point of closest approach (PoCA) algorithm is illustrated in Fig. 4. It is shown in two-dimensional (2D) form for simplicity of presentation, though it is of course a three-dimensional (3D) algorithm. A muon takes a stochastic scattered path through the object volume. We measure scattering in two planes, and estimate particle momentum. Since the scattering is of order ~milliradians, we can approximate the path by a straight line that connects the entry and exit points. Voxels (3D pixels) along the line are candidates for having influenced the ray. We then make the assumption that the scattering occurred due to a single scattering event, and locate the estimated point of scatter by extrapolating the incident and scattered rays to their point of closest approach. This is similar to a nuclear scattering reconstruction technique previously described in Ref. [12]. The information signal for the muon is calculated using Eq. (8). This signal is assigned to the voxel containing the point of closest approach, and we assign zero to the other candidate voxels. As many muons pass through the object volume, we take the mean of the contributions from all muons to each voxel. Each muon thus contributes to the 3D image, eventually filling the voxels with the estimated scattering strength. Because of our ability to extrapolate to the point of closest approach, the algorithm is intrinsically 3D, even before the application of tomographic methods.

We would, of course, expect the PoCA algorithm to work best for volumes containing small, isolated objects, wherein the single scattering assumption is most valid. In the next two sections we will show results obtained using PoCA for such scenes. Later, we will describe continuing development of reconstruction

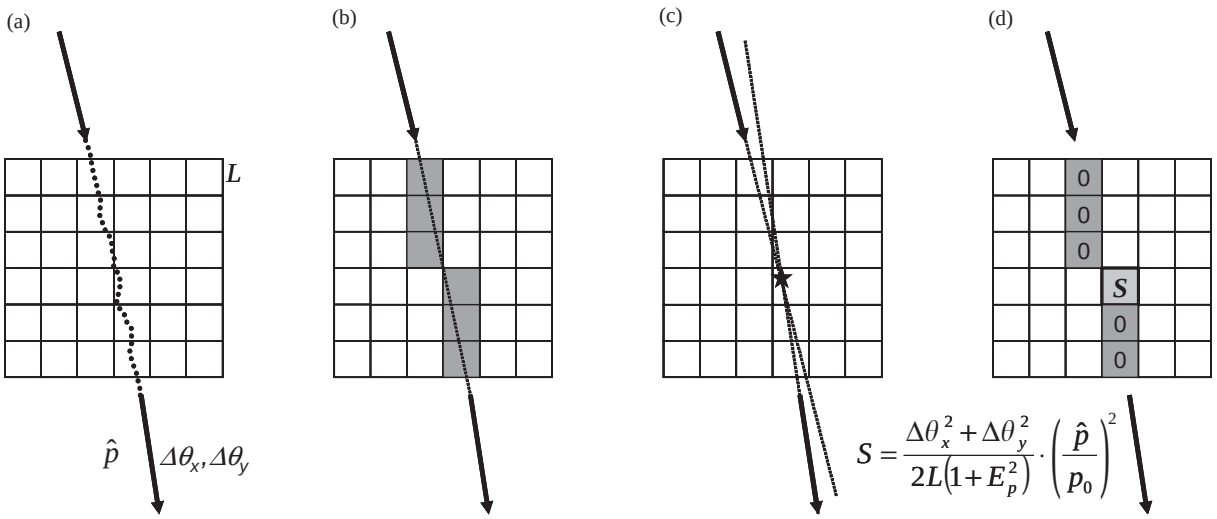

Fig. 4. PoCA reconstruction algorithm, shown in 2D for simplicity. A muon's stochastic path through an object volume (a). We measure scattering in two planes, and estimate particle momentum. Estimate muon path and identify voxels through which ray passed (b). Localize scattering signal to voxel containing PoCA (c). Define scattering signal as shown, and assign signal to the PoCA voxel, 0 to other candidate voxels (d). Take mean signal in each voxel over all muons to establish reconstructed scattering strength.

methods that are less affected by background scatter.

6. Experimental proof of principle

To demonstrate proof of principle, we constructed a small experimental apparatus built with a set of four position-sensitive delay line readout drift chambers [13]. Two groups of detectors, each measuring particle position in two orthogonal coordinates, were placed above an object region and two groups were placed below, according to the configuration shown in Fig. 3, except that no momentum-measuring planes were used. Two plastic scintillators in coincidence with the outermost drift chambers provided a timing trigger required by the delay line detectors. Signals from the detectors were amplified and discriminated in standard NIM electronics, were digitized in FERA ADCs, and read into a computer using a PC-based data acquisition system, PCDAQ [14]. The detectors measured position to a precision of about 400 μm full-width at half-maximum (FWHM), and angles to about 2 mrad FWHM. The solid angle of this apparatus limited event rate to only a fraction of the available muon rate, and the lack of momentum measurement limited precision of object reconstruction, but the device was sufficient for proof of principle.

Two test objects and corresponding cosmic ray muon radiographs of those objects are shown in Fig. 5. These radiographs were produced via the experimental prototype and PoCA reconstruction algorithm described above. The bar-like features appearing above and below the test objects in the radiographs are due to thin-walled steel beams which supported the objects. The steel c-clamp, shown in Fig. 5a, is of similar thickness to the steel beams, so these two features appear with similar intensity in the image. The lead (high-Z) "LANL" letters, shown in Fig. 5b, produce much more scattering than do the beams (medium-Z), so the beams appear fainter in this normalized image. Each of these reconstructions was made using data from about 100,000 muons. The data were collected over several hours; an optimized detector system with high efficiency and large solid angle could acquire as many muons in ~ 30 min. These long runs were made to illustrate the structure of the objects for demonstration purposes. For a simple yes/no detection decision (as in the contraband detection problem outlined in Refs. [8,9]), considerably fewer muons, hence shorter exposure times, would clearly be adequate.

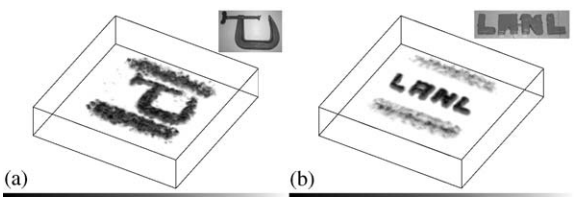

Fig. 5. Experimentally produced cosmic ray muon radiographs of (a) a steel c-clamp, and (b) "LANL" constructed from 1″ lead stock. The bar-like features result from steel beams used to support a plastic object platform.

7. Monte Carlo simulation of material identification

In order to examine how well this technique works for larger, more complex scenarios and to test momentum normalization, we developed a simulation code that generates cosmic-ray muons with the appropriate distribution of energies and angles, propagates them through a test volume, and generates the positions at which they would be detected in four detector planes. The muon spectrum, angular distribution, and rate were appropriate for sea level. We used experimental results for a tungsten block test object to validate our Monte Carlo simulation, as described in Ref. [7].

We illustrate the discrimination of low-, medium-, and high-Z materials via a simple simulated example. We chose a test scene containing three $5 \times 5 \times 5\,\mathrm{cm}^3$ blocks, one constructed of tungsten (high Z), one of iron (medium Z) and one of carbon (low Z). We then simulated the passage of about 100,000 muons through the objects, and through three additional iron plates for measurement of particle momentum. Finally, we applied the PoCA reconstruction algorithm to fill a voxelated 3D volume with scattering strength (λ) estimates.

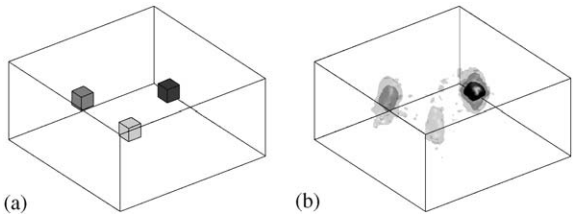

Fig. 6. Discrimination of material Z (simulated). Objects are shown in (a) three $5\times5\times5\,\mathrm{cm}^3$ cubes, one of tungsten (high-Z, shown darkest), one of iron (medium-Z, less dark), and one of carbon (low-Z, shown lightest). A simulated muon radiograph is shown in (b). The position and Z-level of all three objects is clearly represented.

To visualize the reconstructed volume, we defined voxels with $\lambda\geqslant20$ as high-Z material (refer to Fig. 2), $3\leqslant\lambda<20$ as medium Z, and $0.25\leqslant\lambda<3$ as low-Z material. Placement of objects is shown in Fig. 6a. Fig. 6b is a visualization of the momentum-normalized reconstruction, wherein a dark isosurface is drawn around high-Z material, a lighter isosurface around medium-Z material, and a still lighter isosurface around low-Z material. The three blocks are clearly represented in the reconstruction with appropriate Z levels.

The halo effect around the higher density material is due to blurring of the edges of the objects. This blur is mainly due to error in assigning the point of closest approach along the ray path in the PoCA method. As cosmic ray muons tend to probe the volume vertically (particularly for this simulation of an experimental apparatus with limited acceptance angle), the blur is predominantly vertical.

8. High-Z detection algorithm

We have shown in our previous work the feasibility of detection of high-Z material within low-density cargo via cosmic ray muon radiography for the purpose of contraband detection [8,9]. The PoCA reconstruction method works well for modest cargo densities. For instance, in Ref. [8], we illustrated the detection of three small uranium bricks hidden with a cargo of sheep. However, large amounts of medium-Z material (such as a cargo container filled with iron parts) might produce enough blur to prevent the detection of a compact high-Z object with the PoCA reconstruction algorithm.

We have developed a new high-Z detection algorithm is more robust relative to scattering backgrounds. This algorithm exploits the fact that a compact high-Z object tends to produce many highly scattered rays which intersect within a small volume. Though a large depth of medium-Z material can produce highly scattered rays, those rays will be spread over a larger volume. This phenomenon is the basis of a "ray crossing" detection algorithm which works as follows, starting with a list of the scattering muon tracks:

- Eliminate all tracks in which scattering is less than specified value.
- Of the remaining tracks, eliminate all tracks which do not approach another track within a specified distance.
- For each voxel in the reconstructed volume, count the number of ray pairs which have their points of closest approach to one another within that voxel. Normalize each voxel signal by dividing by the original number of rays that passed through that voxel.
- Highlight regions in which the voxel signal exceeds a specified threshold.

We applied this "ray crossing" algorithm to the following simulated scene. A $6\times2.4\times2.4\,\mathrm{m}^3$ cargo container with 3 mm steel walls was filled with about 12 tons of iron, distributed uniformly, to simulate a cargo of iron parts. The bulk density of $0.3\,\mathrm{g\,cm}^{-3}$ represents the load limit for a standard shipping container. Within the iron were buried three $9\times9\times12\,\mathrm{cm}^3$ uranium bricks. We simulated 1 min of cosmic ray muon exposure and processed the simulated muon tracks with our ray crossing algorithm. Fig. 7a is a visualization of the reconstruction of this scene. All three uranium bricks are clearly identified. Fig. 7b shows our control reconstruction, the iron cargo without the hidden bricks. This image is empty of any signal. The ray-crossing algorithm shows great promise to eliminate scattering background. We are continuing its development.

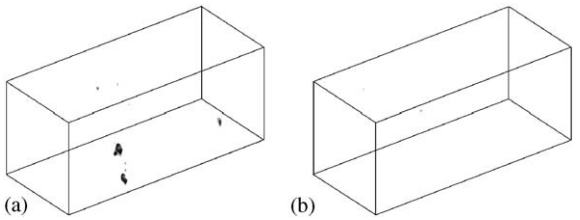

Fig. 7. Reconstructions of 1 min of simulated cosmic ray muon radiography of a $6 \times 2.4 \times 2.4\,m^3$ cargo container containing 12 tons of distributed iron with three buried $9 \times 9 \times 12\,cm^3$ uranium bricks (a) and without uranium bricks (b). These reconstructions were made with a ray-crossing detection algorithm.

9. Summary

We have developed a new technique for radiography using the multiple scattering of cosmic ray muons which is particularly sensitive to high-Z materials. In this paper, we described the theoretical foundations for the technique and presented an experimental proof of principle. We have developed two reconstruction algorithms, one appropriate for the detection and Z discrimination of relatively isolated objects, and another designed for the quick detection of high-Z material obscured by medium- or low-Z material.

Development of this technique is ongoing. The focus of our current efforts is on the development of robust detectors for field applications and on improving reconstruction and analysis techniques. In particular, we are developing a fully tomographic algorithm that incorporates both the scattering and displacement of particles for more precision radiography.

References

[1] K. Hagiwara, et al., Particle data group, review of particle physics, Phys. Rev. D 66 (1) (2002) 1.
[2] E.P. George, Cosmic rays measure overburden of tunnel, Commonwealth Engineer, July 1, 1955, pp. 455–457.
[3] L.W. Alvarez, et al., Science 167 (1970) 832.
[4] S. Minato, Mater. Eval. 46 (1988) 1468.
[5] K. Nagamine, J. Geogr. 104 (7) (1995) 998.
[6] E. Frlez, et al., Nucl. Instr. and Meth. A 440 (2000) 57.
[7] K. Borozdin, et al., Nature 422 (2003) 277.
[8] W.C. Priedhorsky, et al., Rev. Sci. Instr. 74 (10) (2003) 4294.
[9] L.J. Schultz, et al., Cosmic ray muon radiography for contraband detection, in: Proceedings of AccApp'03, San Diego, CA, June 2003, in press.
[10] M. Motiki, et al., Precise measurement of atmospheric muon fluxes at sea level, in: Proceedings of the ICRC 2001, 927, Hamburg, Germany, 2001.
[11] T. Sanuki, et al., Atmospheric muons at various altitudes, in: Proceedings of the ICRC 2001, Vol. 950, Hamburg, Germany, 2001.
[12] G. Charpak, et al., Proc. Soc. Photo-opt. Instrum. Eng. 312 (1983) 156.
[13] C.L. Morris, H.A. Thiessen, G.W. Hoffman, IEEE Trans. Nucl. Sci. NS-25 (1) (1978) 141.
[14] G.E. Hogan, PC DAQ: A Personal Computer Based Data Acquisition System, Los Alamos National Laboratory, Los Alamos, 1998 LA-UR-98-4531.